

Co-funded by the



DISCO

Grant Agreement: 755443

DELIVERABLE D5.2

Defect chemistry and thermodynamics of Cr-doped UO₂ fuels: Model development and applications (Mid-term report)

Enzo Curti and Dmitrii Kulik

(Laboratory for Waste Management, Paul Scherrer Institut)

Date of issue of this report: **14/05/2019**

Report number of pages: 29

Start date of project: **01/06/2017**

Duration: 48 Months

Project co-funded by the European Commission under the Euratom Research and Training Programme on Nuclear Energy within the Horizon 2020 Framework Programme
Dissemination Level

PU Public
PP Restricted to other programme participants (including the Commission Services)
RE Restricted to a group specified by the partners of the Disco project
CO Confidential, only for partners of the Disco project

X

Table of Contents

1	Introduction	3
2	Selection and testing of thermodynamic data	4
2.1	The HERACLES database.....	4
2.2	Selection and testing of data for Cr	4
2.3	Implementation in GEM-Selektor	6
3	Defect and coordination chemistry of Cr-doped UO₂	8
3.1	UO ₂ structure and oxygen defects in UO _{2+y}	8
3.2	Coordination of Cr in UO ₂ inferred from coordination chemistry	10
3.3	Cr ³⁺ defect formation in stoichiometric urania (UO ₂)	11
3.4	Cr ³⁺ defect formation in hyperstoichiometric urania (UO _{2+y})	12
3.5	Solubility of Cr(III) in stoichiometric UO ₂ calculated from defect equilibria	14
4	Development/application of a solid solution model for Cr-doped UO₂	18
4.1	Preliminary remarks	18
4.2	Definition of end-members.....	18
4.3	Implementation in GEM-Selektor and model calibration	19
4.4	Fuel oxygen potential calculations	22
4.5	Outlook	24
	References	25
	Appendix 1 – Calculation of Cr(III) solubility in UO₂ based on defect equilibria	28

1 Introduction

The EURATOM Project “DisCo” (modern spent fuel **D**issolution and chemistry in failed **C**ontainer conditions), carried out within the Horizon2020 framework program, is a collaborative effort among European partners aiming at increasing the knowledge on spent fuel dissolution under repository-relevant conditions (highly reducing conditions). Experimental work will focus on dissolution studies of so-called “modern” fuels, i.e. fuels doped with alumina/chromia or mixed oxide fuels (MOX). Both types of fuels are increasingly used in light water reactors in order to optimize energy harvesting. The dopants trigger grain growth during sintering of the UO_2 pellets, reducing fission gas release and therefore allowing higher power rates to be achieved during reactor operation.

Currently, the behaviour of modern fuels under geological storage conditions is still largely unknown. One of the major objectives of DisCo is thus to obtain leach data on these fuels and to compare their dissolution behaviour to that of conventional UO_2 fuels under geological storage conditions. The focus of the project is on matrix dissolution rather than on radionuclide release.

Modern fuels reach higher burnups than conventional UO_2 fuels. This could lead to different microstructural features and consequently to different accessibility of water to leachable radionuclides. Another issue is the effect of compositional changes induced by the addition of the dopant itself and the larger amount of fission products produced due to the increased burn-up. These changes may potentially lead to higher fuel oxygen potentials, which eventually might cause the oxidation of long-lived fission products such as ^{99}Tc , ^{126}Sn , ^{79}Se , ^{93}Mo and of redox sensitive actinides, making them more soluble and leachable under repository conditions.

This contribution is entirely dedicated to the theoretical assessment of oxygen potentials in irradiated modern fuels, specifically Cr-doped UO_2 fuels, by means of a comprehensive thermodynamic treatment. In this report, we develop and apply a thermodynamic model for UO_2 fuels including equilibrium with $\text{Cr}_2\text{O}_3\text{-UO}_2\text{-U}_4\text{O}_9$ solid solution and with separate pure phases for fission products, Pu and minor actinides. The model is based on current evidence arising from defect chemistry on the substitution mechanisms of Cr(III) and U(V) in UO_2 and is calibrated against experimental data from the literature. It is implemented in the GEM-Selektor (PSI) code using the in-house database HERACLES (see details in the next sections).

In the next project year, we will then expand the U-oxide solid solution model by including elements known to be soluble in the UO_2 matrix (Pu, minor actinides and lanthanides) and attempt to define additional solid solutions for minor phases formed during reactor irradiation (metallic ϵ -phase, “grey phase”). In addition, we plan to study the effects of burn-up evolution and internal Zircaloy oxidation on the oxygen potential.

2 Selection and testing of thermodynamic data

2.1 The HERACLES database

In the past years, efforts have been made at Paul Scherrer Institut (PSI) to select thermodynamic data for solids, liquids and gaseous phase, covering most elements relevant to nuclear fuels and fission products under in-pile and dry storage conditions. This resulted in an extensive database called HERACLES-TDB (<https://www.psi.ch/heracles/gems-specific-heracles-database>) integrated in the in-house chemical code GEM-Selektor (<http://gems.web.psi.ch/>) (Kulik et al., 2013). The database includes standard molar thermodynamic properties for compounds of actinides, of fission products, and of minor actinides, covering almost all elements of interest. Presently, data are available for over 610 condensed compounds and over 360 gaseous species. Data selection was carried out using a large number of references, listed in the aforementioned homepage of the HERACLES project.

Unfortunately, chromium, an element of major interest for the DisCo project as it is the most common dopant in modern fuels, was not included in the original data compilation. Therefore, a preliminary task of PSI's contribution was the selection of key thermodynamic data for this element and their integration into the GEM-Selektor code.

2.2 Selection and testing of data for Cr

A set of Cr data judged to be critical for our task within the DisCo project was selected. We started by reviewing the source data reported by Jeannin et al. (1963) and Toker et al. (1991). The focus was on the key equilibrium between eskolaite (Cr_2O_3) and metallic Cr at temperatures below melting, since this reaction would buffer oxygen partial pressures if *both* phases were present at equilibrium in the fuel. Unfortunately, the cited references do not include temperature dependent heat capacity data, which are necessary to carry out thermodynamic calculations at any given temperature of interest. Heat capacities were taken from the comprehensive compilation of Barin (1989), after verifying that the free energies compiled in the latter database are consistent with those given in Jeannin et al. (1963) and Toker et al. (1991). In order to include them in GEM-Selektor, heat capacities had to be interpolated to obtain the coefficients for the following 10-term equation used in the code:

$$c_p(T) = a_0 + a_1T + a_2T^{-1} + a_3T^{-0.5} + a_4T^2 + a_5T^3 + a_6T^4 + a_7T^{-3} + a_8T^{-1} + a_9T^{-0.5}$$

Tables 1 and 2 list the selected standard state (298.15 K, 1 bar) thermodynamic data for chromium solids (molar Gibbs free energy, molar entropy and heat capacity coefficients). These data were added to the HERACLES database and implemented into the GEMS-Selektor code. They build the basis for the calculations involving chromium presented in the next chapters.

Table 1- Selected thermodynamic data for chromium solids

Property	Cr ₂ O ₃	Cr	CrO ₂	CrO ₃	CrI ₂	CrI ₃
$\Delta_f G^0$ (kJ mol ⁻¹)	-1057.9	0	-544.84	-512.51	-165.56	-205.47
S^0 (J mol ⁻¹ K ⁻¹)	81.199	23.64	51.045	73.22	169.034	199.577
c_p^0 (J mol ⁻¹ K ⁻¹)	117.563	23.2385	99.6717	69.326	73.679	111.675
a ₀	118.3	32.3349	94.5583	82.5486	66.9438	105.437
a ₁	0.0099	-0.01589	0.01715	0.02168	0.02259	0
a ₂	-1.4 x 10 ⁶	-542904	13.2353	-1.75x10 ⁶	0	0
a ₃	0	0	0	0	0	0
a ₄	0	2.1 x 10 ⁻⁵	0	0	0	0
a ₅	0	-4.46 x 10 ⁻⁹	0	0	0	0
a ₆	0	0	0	0	0	0
a ₇	0	0	0	0	0	0
a ₈	0	0	0	0	0	0
a ₉	0	0	0	0	0	0

Table 2 - Selected thermodynamic data for chromium gas species

Property	Cr(g)	CrO(g)	CrO ₂ (g)	CrO ₃ (g)
$\Delta_f G^0$ (kJ mol ⁻¹)	352.62	154.63	-87.311	
S^0 (J mol ⁻¹ K ⁻¹)	174.306	239.267	269.224	
c_p^0 (J mol ⁻¹ K ⁻¹)	20.7901	31.3316	43.3263	
a ₀	21581.2	64.228	40.5625	66.7745
a ₁	6.68684	0.00784	0.03006	0.02175
a ₂	-2.45743 x 10 ⁸	-1.67675 x 10 ⁶	-413342	-1.48 x 10 ⁶
a ₃	-442123	-569.757	0	0
a ₄	-6.77344 x 10 ⁻⁴	-6.62987 x 10 ⁻⁷	-1.86 x 10 ⁻⁵	-1 x 10 ⁻⁵
a ₅	7.65224 x 10 ⁻⁸	7.75564 x 10 ⁻¹¹	3.95 x 10 ⁻⁹	1.52 x 10 ⁻⁹
a ₆	-4.62271 x 10 ⁻¹²	-4.25608 x 10 ⁻¹⁵	0	0
a ₇	1.21458 x 10 ¹⁰	2.4525 x 10 ⁸	0	0
a ₈	4.18341 x 10 ⁶	5621.34	0	0
a ₉	-556.889	-0.66168	0	0

Test calculations were carried out to check the selected data. We focussed on the Cr-Cr₂O₃ equilibrium, because, as already noted, metallic Cr and eskolaite may act as oxygen partial pressure buffer. Moreover, these data will be used to define properties of Cr-end members in the solid solutions developed later. In order to test the consistency of calculations with experimental data, we carried out simple GEM-Selektor computations, in which excess amounts of pure metallic chromium and Cr₂O₃ were equilibrated with increasing amounts of oxygen. These calculations were then compared to the available experimental data on

equilibrium p_{O_2} for the Cr-Cr₂O₃ equilibrium. The results of this comparison are summarized in Fig. 1, which shows the data from Toker et al. (1991) and Povoden et al. (2006) together with calculations obtained from two alternative selections for the standard properties of Cr₂O₃. The blue line was obtained using the data of Barin (1989), whereas the green line (Cr₂O₃-bis) was obtained using standard properties derived from the optimization of Povoden et al. (2006) data. It is evident that the two choices lead only to minor differences. Because all heat capacities used stem from Barin's compilation, we decided for consistency reason to use only properties listed in Barin (1989) for all GEM-Selektor calculations related to the present study.

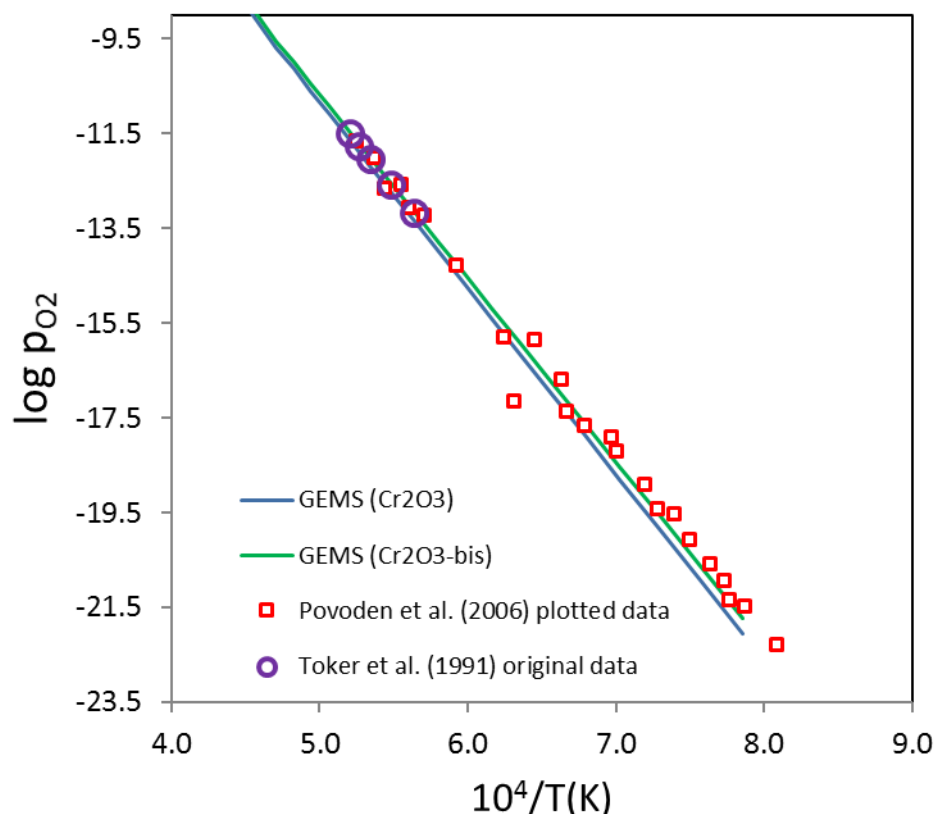


Fig. 1 – Comparison of experimental data and GEM-Selektor calculation for the equilibrium between pure chromium metal and pure Cr₂O₃ (eskolaite).

2.3 Implementation in GEM-Selektor

The gas phase is treated as an ideal mixture of ideal gases, whereas a variety of mixing models is available to model melts and solid solutions. For each compound and gas species, the molar enthalpy of formation from the elements at their standard states, absolute entropy and heat capacity at standard state ($T_r = 298.15$ K and $P_r = 1$ bar) were specified in GEM-Selektor's *DComp* module. The molar Gibbs energy of formation was then calculated internally from the aforementioned quantities. Auxiliary thermodynamic data were taken from Cox et al. (1989). In Fig. 2, such implementation is shown for Cr₂O₃ (two variants) and Cr metal.

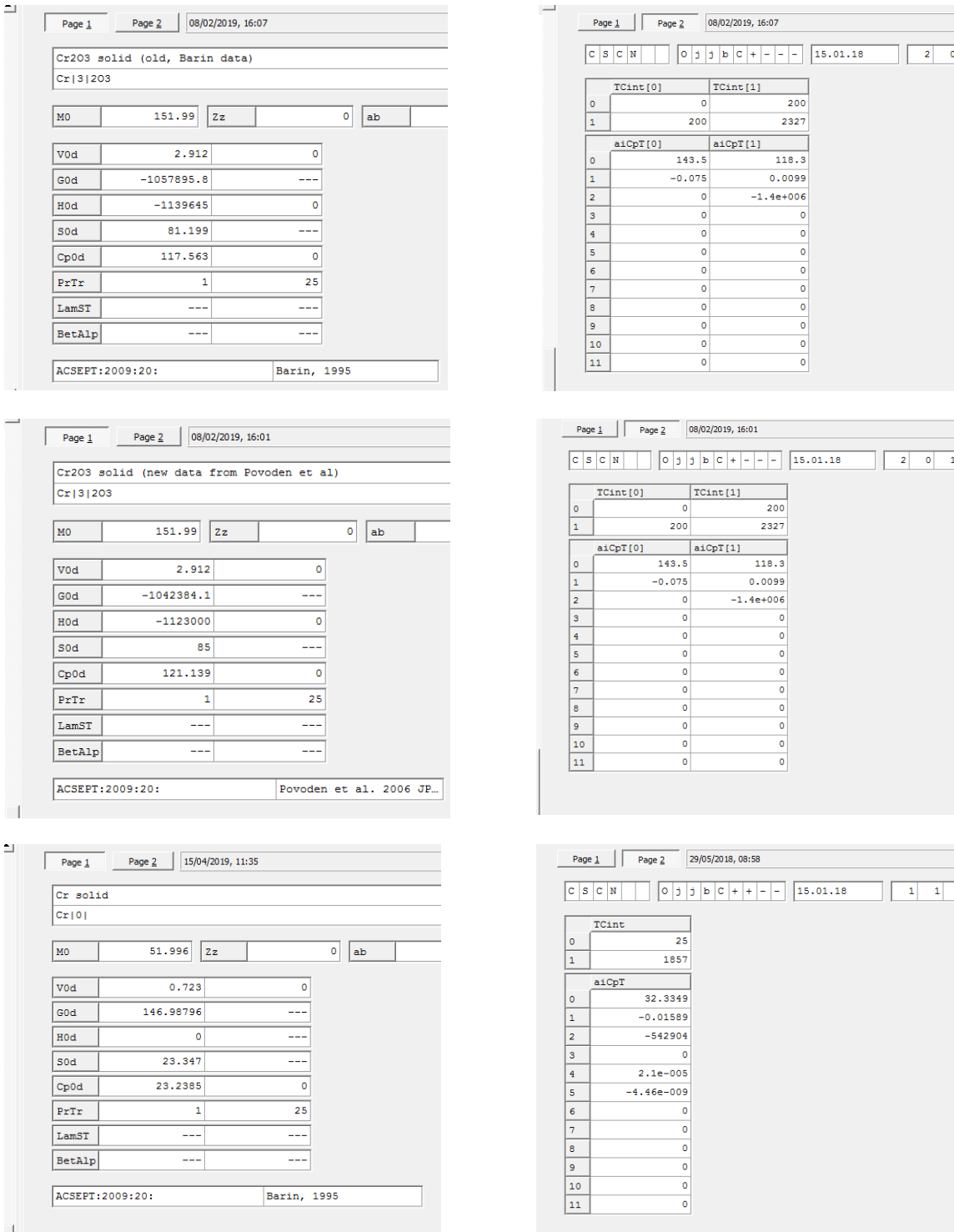


Fig. 2 – Implementation of thermodynamic properties for Cr_2O_3 (in two variants, see text) and metallic Cr in the GEM-Selektor code. Left column: standard state properties: $M0$ =molar weight (g/mol), $V0d$ = molar volume (J/bar), $G0d$ =Gibbs free energy (J/mol), $H0d$ =enthalpy (J/mol), $S0d$ =entropy (J mol⁻¹ K⁻¹), $Cp0d$ = heat capacities (J mol⁻¹ K⁻¹), $PrTr$ = standard state pressure (bar) and temperature (°C). Right column: temperature range and coefficients for $Cp(T)$ extrapolation.

3 Defect and coordination chemistry of Cr-doped UO₂

Before tackling the challenge of deriving a thermodynamic solid solution model for Cr-doped UO₂ fuel, in this chapter the crystal chemistry of stoichiometric and hyperstoichiometric uranium oxide with minor amounts of incorporated Cr is reviewed, with particular attention to defect chemistry studies. The aim is to use this information for the definition of *realistic* solid solution end-members and exclude those not consistent with evidence derived from defect and coordination chemistry.

3.1 UO₂ structure and oxygen defects in UO_{2+y}

Uranium (IV) oxide adopts the fluorite structure, which is typical for compounds having a cation/anion radius ratio close to unity and MX₂ stoichiometry. The crystal lattice of stoichiometric UO₂ is characterized by a cubic close-packed *cationic sublattice* (U⁴⁺), which defines a face-centered primitive cell with all eight tetrahedral interstices fully occupied by anions (O²⁻) (Fig. 3a). The oxygen anions inscribe a cube in the interior of the unit cell with a cation vacancy (V) in the centre. They build an infinite 3-dimensional network of equally sized face-shared cubes, the *anionic sublattice* (Fig. 3b). The half of these O-cubes host 8-fold coordinated U⁴⁺ cations, the other half is vacant. In the jargon of defect chemistry, the unfilled cubes are called *interstitial sites*. They define a *vacancy* or *interstitial sublattice*, in addition to the aforementioned cationic and anionic sublattices.

In contrast to more compact crystal structures (e.g. NaCl-type), the fluorite structure is relatively open, offering space for hosting a variety of foreign ions and facilitating ionic diffusion (Smyth, 2000, p. 13). Specifically, oxygen diffusion through the interstitial sublattice of UO₂ appears to be the main driving force for the formation of hyperstoichiometric urania (Yu et al., 2015). This is ultimately the reason for the observed strong dependence of UO₂ hyperstoichiometry on oxygen partial pressure. As molecular oxygen diffuses into the UO₂ lattice, it picks up electrons and is incorporated as O²⁻ in the interstitial sites, thereby oxidizing U⁴⁺ to U⁵⁺ (not U⁶⁺ as we will see later).

An alternative mechanism for the formation of hyperstoichiometric UO₂ is charge compensation via creation of U⁴⁺ vacancies (1 U⁴⁺ vacancy for each 2 interstitial O²⁻ created), however, this mechanism seems to be far less significant due to the much lower diffusivity of U compared to O (Middleburgh et al., 2012). Hypostoichiometry, contrary to PuO₂, is more difficult to achieve in pure UO₂ and requires elevated temperatures in excess of 1300 °C (Olander, 1976, p.146).

It may surprise that interstitial oxygen resides in an environment coordinated by 8 other oxygen ions, as this should lead to strong electrostatic repulsion. However, one has to realize that O-O distances are relatively large (3.56 Å) and that repulsion is strongly mitigated by the high charge provided by 6 U⁴⁺ in the second shell at 4.12 Å distance (octahedral coordination).

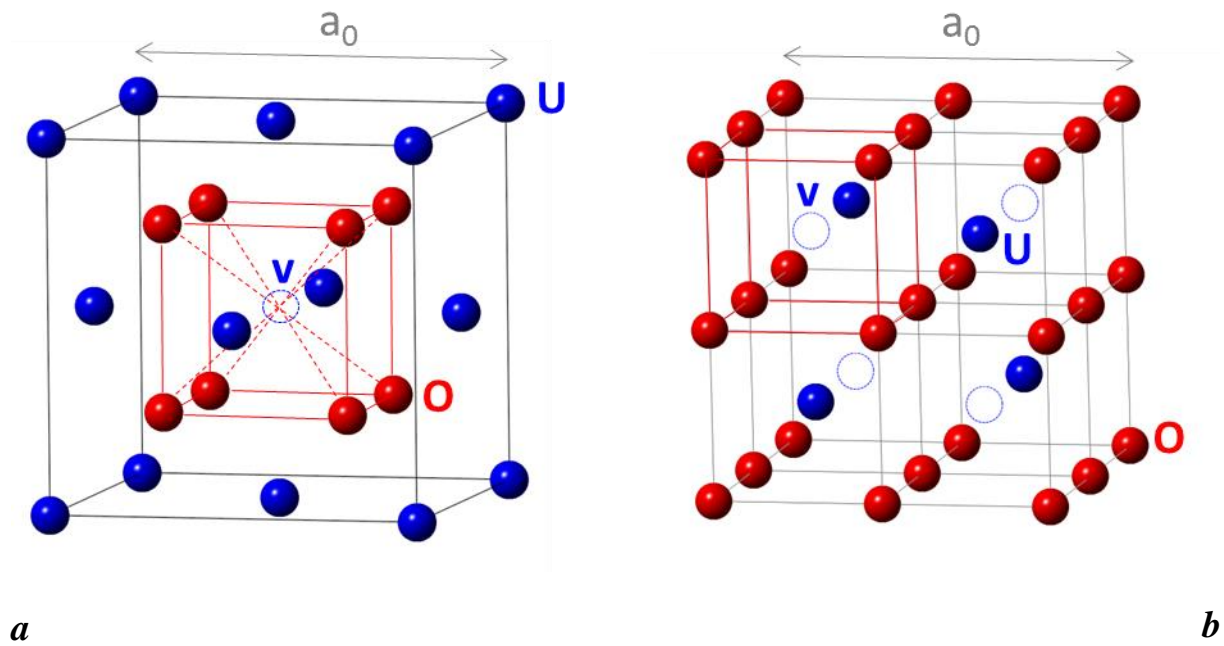


Fig. 3 – Visualization of the stoichiometric UO_2 crystal structure: (a) elemental cell; (b) anionic sublattice. See text for more explanation.

Furthermore, at high degrees of hyperstoichiometry interstitial oxygen forms defect complexes in off-centered positions (Olander, 1976, p.148; Willis, 1978; Wang et al. 2014). Willis (1978) states that for $y < 0.01$ in UO_{2+y} excess oxygen occupies U^{4+} -equivalent interstitial positions. At higher values of y the so-called 2:2:2 (Willis or di-interstitial) defect complex forms, consisting of two interstitial oxygens occupying juxtaposed vacancies and two regular oxygen ions shifted along the (1 1 1) direction.

Several experimental and simulation studies (Wang et al 2014, Prieur et al. 2013, Prieur et al. 2018) indicate that U^{4+} is oxidized to U^{5+} , not to U^{6+} . At low temperature, U^{5+} occupies U lattice positions adjacent to O^{2-} interstitials, while at high temperature (>1200 K) the U^{5+} distribution is random. This means ordered U^{5+} at $T < 1200$ K and complete disorder at $T > 1200$ K. The entropy of mixing of the two clusters will thus differ.

Another study that gives insight in the formation of O defect clusters in UO_2 is the work of Elorrieta et al. (2016). These authors determined, based on discontinuities of XRD and Raman data, different O interstitial complexes as a function of x in UO_{2+x} (citation):

"(i) up to $UO_{2.05}$, a progressive incorporation of oxygen atoms as point defects within interstitial sites occurs; (ii) between $UO_{2.05}$ and $UO_{2.11}$, these point defects start to rearrange into ordered defect structures or Willis clusters; (iii) at around $UO_{2.11}$, part of the Willis clusters start to develop into more densely packed cuboctahedral clusters; (iv) finally, a complete rearrangement of the oxygen atoms in cuboctahedral clusters at $UO_{2.20}$ leads to a new fully ordered superstructure containing oxygen vacancies (U_4O_{9-y})"

3.2 Coordination of Cr in UO₂ inferred from coordination chemistry

According to the HSAB classification (Pearson, 1968) chromium is a hard metal, thus the ionic "hard sphere model" can be used to apply the well-known empirical rules for ionic crystals derived by Pauling (1929).

Table 3 lists the crystal radii of Cr species and their ratio to the radius of O²⁻, compared to the minimum ratios required to stabilize a given coordination geometry according to the first Pauling rule. The values, based on crystal radii taken from Shannon (1976), are listed in order of increasing cation/anion ratio. Ionic charges larger than +3 were neglected, since XAS data indicate that they do not occur in Cr-doped UO₂. Cations such as Cr⁵⁺ and Cr⁶⁺ are anyway too small to be stabilized in the large regular and interstitial cavities of the UO₂ structure.

From inspection of Table 3, it is clear that only Cr²⁺ and Cr³⁺ ions could conceivably be hosted in UO₂, occupying regular U⁴⁺ sites or interstitial sites with oxygen coordination numbers VI, VII or VIII. Incorporation of metallic Cr can be excluded since it would require CN=XII, which is hardly feasible in the UO₂ structure. For Cr²⁺ the ideal coordination number would be VIII, which would make it suitable to be hosted in the cationic and interstitial sublattices of UO₂.

Table 3 – List of crystal radii for Cr species and their ratio to the radius of tetrahedrally coordinated O²⁻ (1.24 Å), compared to the minimum radius ratio necessary to stabilize a given coordination number and corresponding geometry. For Cr²⁺, low spin (LS) and high spin (HS) electronic configurations are distinguished. Radii are taken from Shannon (1976), except for metallic Cr.

Cr species	Radius [Å]	Cr/O radius ratio	Minimum radius ratio	Coordination number	Polyhedron
			0.414	VI	octahedron
			0.592	VII	capped octahedron
Cr³⁺	0.755	0.609			
			0.645	VIII	square antiprism
Cr²⁺ LS	0.87	0.702			
			0.732	VIII	cube
Cr²⁺ HS	0.94	0.758			
			1.000	XII	cubeoctahedron
Cr⁰	1.40	1.129			

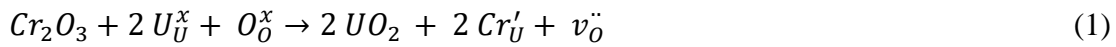
The usual coordination number of Cr³⁺ by oxygen is VI (e.g. in Cr₂O₃, CrOOH, FeCr₂O₄). According to Pauling's 1st rule CN=VII is also possible, however not CN=VIII. Therefore, hosting Cr³⁺ in U⁴⁺ sites or interstitials requires a decrease in the number of first-shell coordinating oxygen ions from VIII to VII or VI. It must be emphasized that Cr³⁺ has the highest crystal field stabilization energy (CSFE) of all d-series transition metals (Stubican and

Greskovich, 1975) hence it has the strongest tendency among transition metals to assume octahedral coordination.

Experimental work based on X-ray absorption spectroscopy provides evidence that the dominant form of chromium in UO_2 is Cr(III) (Riglet-Martial et al., 2014; Mieszczyński et al., 2014). Nevertheless, the presence of Cr^{2+} cannot be excluded based on the limited energy resolution of these data.

3.3 Cr^{3+} defect formation in stoichiometric urania (UO_2)

When dealing with Cr(III) dissolution in *stoichiometric* UO_2 , one can take advantage of work performed on the well-studied $\text{ZrO}_2\text{-Y}_2\text{O}_3$ system (yttria-stabilized zirconia). This system is to some extent a chemical analogue of Cr-doped stoichiometric UO_2 , since the dopant is a trivalent cation and tetravalent zirconium cannot be oxidized or reduced in oxides. Neutron diffraction data and *ab initio* calculations (Goff et al. 1999; Parkes et al. 2015) indicate that the charge-compensating mechanism upon substitution of trivalent Y in Zr_2O is the formation of oxygen vacancies in the anionic sublattice. For each pair of U^{4+} cations replaced by two Y^{3+} cations, one oxygen vacancy is formed. We may therefore postulate the following defect formation reaction for Cr(III) in stoichiometric UO_2 (we use here the standard Kröger-Vink notation, see e.g. Smyth, 2000) :



This mechanism is consistent with the results of atomistic simulations (Middleburgh et al. 2012; Guo et al. 2017). At very low dopant levels the concentrations of regular U and O sites is close to unity. Therefore, under the premise that there are no other significant sources of Cr or O defects, the equilibrium constant of reaction (1) can be approximated by:

$$K(T) \cong x_{\text{Cr}'_\text{U}}^2 x_{v_\text{O}^\bullet} = x_{\text{Cr}'_\text{U}}^2 \times \frac{1}{2} x_{\text{Cr}'_\text{U}} = \frac{1}{2} x_{\text{Cr}'_\text{U}}^3 \quad (2)$$

where the symbol x denotes mole fractions normalized to U-sites. This leads to the following expression for the equilibrium concentration of Cr(III) in stoichiometric UO_2 :

$$x_{\text{Cr}'_\text{U}} = \sqrt[3]{2 K(T)} \quad (3)$$

The concentration of oxygen vacancies was eliminated in eq. (2) by noting that one oxygen vacancy is formed for each pair of Cr^{3+} ions. From eq. (3), one may thus determine the equilibrium concentration of Cr in stoichiometric UO_2 if $K(T)$ is known. Determination of $K(T)$ requires either direct measurements or the knowledge of the enthalpy of defect formation with the corresponding entropy contribution (see Smyth, 2000, chapter 3). This calculation will be shown later in this chapter.

Note that no free oxygen appears in reaction (1), therefore $x_{\text{Cr}'}$, the equilibrium Cr^{3+} mole fraction in *stoichiometric* UO_2 , is $p\text{O}_2$ -independent. In other words, Cr(III)-doping in

stoichiometric UO_2 fuel via this defect formation mechanism has no influence on oxygen potential and *vice versa*. We postulate, in agreement with Middleburgh et al. (2012) that reaction (1) is indeed the governing mechanism during the fabrication of Cr-doped fuel, since synthesis conditions are kept reducing (H_2/CO_2 atmosphere) in order to avoid any hyperstoichiometry (Arborelius et al., 2006).

The substitution expressed by reaction (1) is shown schematically and unrelaxed in Fig. 4 as one of many possible configurations. The oxygen vacancy is placed purposely midway between the two Cr^{3+} ions in order to minimize local charge imbalance. This arrangement corresponds to the "fixed configuration" identified using atomistic simulations by Guo et al. (2017) to be the energetically most favourable.

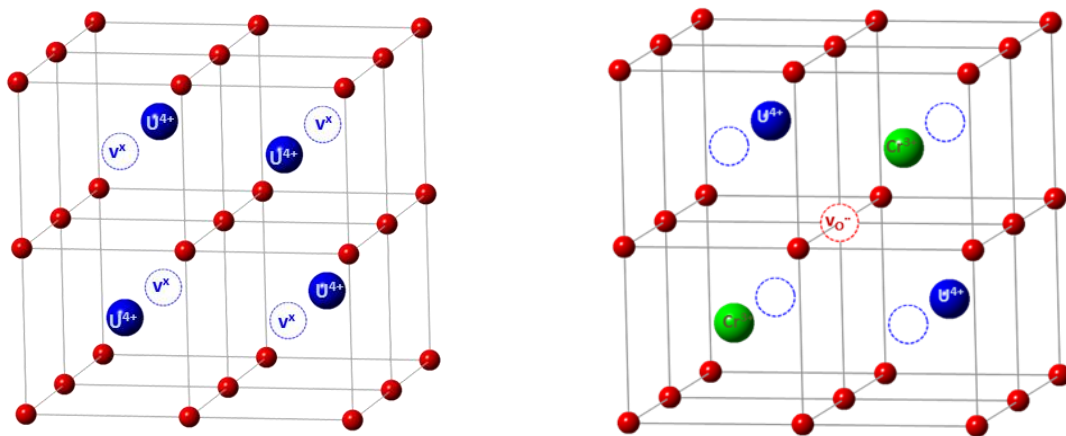


Fig. 4 – Substitution mechanism of Cr(III) (schematic) in stoichiometric UO_2 . The left side shows the undisturbed UO_2 anionic sublattice, the right side the same sublattice after the substitution.

Note that the substitution mechanism illustrated in Fig. 4 is consistent with 1st Pauling rule, as the creation of an oxygen vacancy adjacent to the Cr^{3+} ions reduces the oxygen coordination number from VIII to VII. $\text{CN}=\text{VII}$ is compatible with the crystal radius of Cr^{3+} , whereas $\text{CN}=\text{VIII}$ would be an unstable configuration.

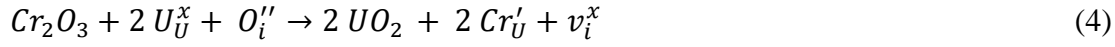
Other conceivable Cr(III) substitutions in stoichiometric UO_2 have been postulated, e.g. the formation of a defect cluster consisting of 3 Cr^{3+} replacing 3 U^{4+} plus 1 Cr^{3+} occupying an interstitial site. However, the formation of this complex appears to be energetically unfavourable after Middleburgh et al. 2012.

3.4 Cr^{3+} defect formation in hyperstoichiometric urania (UO_{2+y})

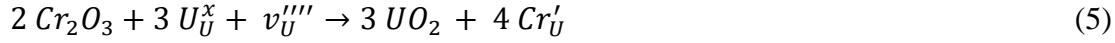
As already discussed in Section 3.1, in-diffusion of molecular oxygen into UO_2 at high $p\text{O}_2$ leads to hyperstoichiometric urania (UO_{2+y}). As for stoichiometric UO_2 , it is possible to

postulate Cr-substitution mechanisms for hyperstoichiometric urania. Middleburgh et al. (2012) proposed the following two reactions:

(A) replacement of 2 U⁴⁺ by 2 Cr³⁺, charge-balanced by eliminating 1 interstitial oxygen¹:



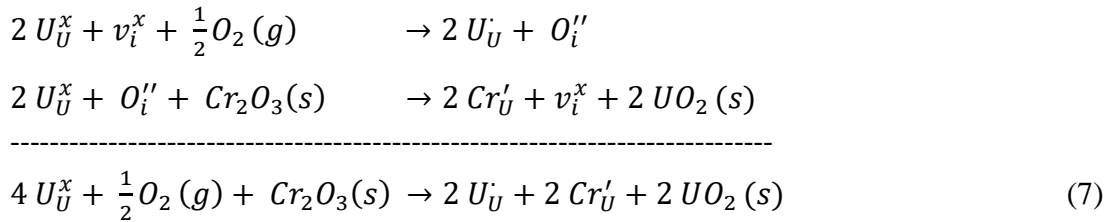
(B) replacement of 3 U⁴⁺ ions and 1 U⁴⁺ vacancy by 4 Cr³⁺ ions:



Based on DFT calculations, reaction (4) appears to be energetically favoured compared to reaction (5), which is the same mechanism already mentioned to be unfavourable in stoichiometric urania. As noted earlier, this mechanism is unfavourable due to the low diffusivity of U compared to O. Therefore, reaction (5) can be neglected. In order to couple reaction (4) with the oxygen partial pressure, one has to consider the equilibria leading to formation of interstitial oxygen in hyperstoichiometric UO₂. The formation of mono-interstitial oxygen defects can be formulated as follows (see eq. 8 in Garcia et al., 2017):



Combining reactions (4) and (6) results in the following *pO₂*-dependent equilibrium, leading to the elimination of all interstitial sites in the net reaction (the greyed out species cancel out):



The equilibrium constant of reaction (7) can be approximated by:

$$K_{AC}(T) \cong x_{Cr'_U}^2 x_{U_i}^2 p_{O_2}^{-1/2} = K_{11} K_{Oi} \quad (8)$$

where *K₁₁* is the equilibrium constants of reaction (4), which can be derived using Middleburgh et al. (2012) defect formation enthalpy, and *K_{Oi}* is the equilibrium constant for reaction (6), given by Garcia et al. (2017).

In contrast to reaction (4), reaction (7) implies a dependency on oxygen partial pressure. This substitution is illustrated in Fig. 5. Locally, the two incorporated Cr³⁺ ions are charge-balanced by nearby pentavalent uranium ions (previously produced through oxidation via transformation of in-diffusing O₂(g) to interstitial O²⁻). For each pair of Cr³⁺ ions incorporated, 1 oxygen interstitial is annihilated, as evidenced in reaction (4).

¹ This reaction corresponds to Eq. (11) in Middleburgh et al. (2012). Note that we added a vacant interstitial (*v_i^x*, not specified in Middleburgh et al., 2012) in order to preserve the site balance.

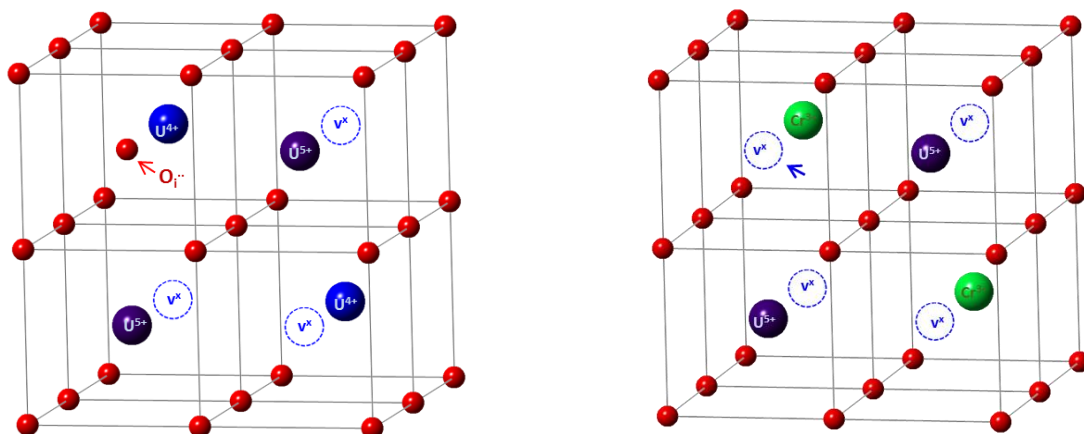


Fig. 5 – Schematic substitution mechanism of Cr(III) in hyperstoichiometric urania. The left side shows the UO_{2+y} anionic sublattice with 2 U^{5+} cations, charge-balanced by 1 interstitial O^{2-} anion (see arrow), the right side shows the same sublattice after substitution of 2 U^{4+} by 2 Cr^{3+} . The interstitial oxygen must be eliminated to preserve local charge balance.

3.5 Solubility of Cr(III) in stoichiometric UO_2 calculated from defect equilibria

In the preceding Section, the dominant substitution mechanisms of Cr(III) have been identified, based on a review of the literature supported with simple crystal chemistry principles. This led to equilibrium expressions for defect-involving reactions, from which the solubility of Cr(III) in both stoichiometric and hyperstoichiometric urania can be in principle derived (reactions 1 and 4, respectively). The amount of Cr in doped LWR fuels will nevertheless be determined by the conditions imposed during fuel synthesis. These are selected so that strictly stoichiometric compositions will result for pure UO_2 ($O/M=2.00$, $M=U$) and hypostoichiometric for Cr-doped UO_2 ($O/M < 2.00$, $M=U+Cr$)².

Therefore, the amount of Cr dissolved in the fuel during synthesis will be limited by reaction (1), not by reaction (4). Since there is no other source of Cr in the system after synthesis (no significant Cr fission product exists) and the vapour pressure of Cr-solids is negligible, the Cr-amount present in the fuel at any time during irradiation can be considered to be fixed by the initial dopant concentration. It will not change, even if the fuel should become hyperstoichiometric. In other words, the Cr-content in the fuel can be treated as a constant and no further equilibration with external sources of Cr(III) needs to be assumed when modelling the thermodynamics of Cr-doped spent fuel. This is the usual approach adopted when modelling extrinsic defects in solids (Smyth, 2000; Garcia et al. 2017). The solubility of Cr(III) in stoichiometric UO_2 at synthesis temperature (about 1800 °C) will thus determine the maximum

² When Cr-doped fuel is synthesized under reducing conditions (preventing the formation of oxygen interstitials), oxygen vacancies will form and thus cause the Cr-doped fuel to become hypostoichiometric.

possible content of Cr in the fuel at any time, since care is taken to select sintering conditions slightly below saturation.

We therefore present here only calculations to determine the solubility of Cr(III) in stoichiometric UO₂. Our calculations follow the approach taken by Motta and Olander (2017) and are developed in detail in Appendix 1. Using this method, a final solution for the equilibrium mole fraction of Cr in stoichiometric UO₂ identical to equation (3) was obtained, along with exact expressions for the concentrations of oxygen defects and regular U and O site occupancies.

The equilibrium constant $K(T)$ for reaction (1) was evaluated using the enthalpy of defect formation derived by Middleburgh et al. (2012) for randomly distributed Cr' and $v_{O\cdot}$ defects ($\Delta H_r = +3.05$ eV/defect = 294.28 kJ/mol). Using standard thermodynamic relations (e.g. Smyth, 2000; Garcia et al. 2017), one obtains:

$$\log K(T) = -\frac{\Delta G_r}{\ln(10)k_b T} = \frac{T\Delta S_r - \Delta H_r}{\ln(10)k_b T} \quad (9)$$

where ΔG_r , ΔS_r and ΔH_r are the free energy, entropy and enthalpy of the defect formation reaction (in eV) and k_b, T are Boltzmann's constant and absolute temperature, respectively. In estimating defect equilibrium constants, the entropy change ΔS_r is usually unknown, so it is customary to neglect the ΔS_r term in eq. (9) and equate ΔH_r with ΔG_r . Typical values of $\Delta S_r/k_b$ are however known to range between 0 and 10, which results in uncertainties as large as four orders of magnitude in the equilibrium constant. Therefore, neglecting entropy contributions can lead to considerable errors.

Here, we use an empirical approach to obtain an estimation of the entropy term by fitting published experimental Cr-solubility data. This approach is shown in Fig. 6 where the Cr(III) solubilities in UO₂ measured within the stability field of Cr₂O₃ (i.e. avoiding the data including equilibrium with other Cr phases) are plotted against Cr(III) concentrations in UO₂ predicted using equations (3) and (9). The experimental data were taken from Riglet-Martial et al. (2014), who also included earlier measurements by Leenaers et al. (2003) and Bourgeois et al. (2001).

The data were first compared with the equilibrium constant predicted assuming $\Delta H_r = \Delta G_r = +3.05$ eV from Middleburgh et al. (2012) and $\Delta S_r/k_b = 0$. The so-defined mass-action-law model underpredicts the measured Cr-solubility data ("zero entropy" model, broken line in Fig. 6). The model was then adjusted by varying the entropy value until the experimental data were fitted satisfactorily ("fitted entropy" model, continuous line). This procedure yielded $\Delta S_r/k_b = 1.4$ ($\Delta S_r = 11.64$ J K⁻¹ mol⁻¹). The corresponding equilibrium constants calculated from eq. (9) are plotted in Fig. 7 and the thermodynamic data derived for the refined model summarized in Table 4.

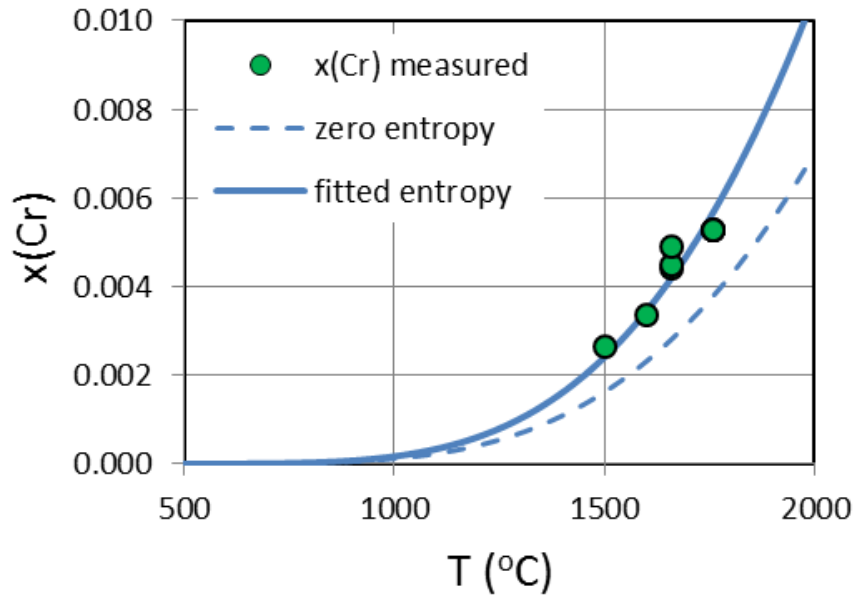


Fig. 6 – Solubility of Cr(III) in stoichiometric UO_2 expressed as mole fraction relative to U sites as a function of temperature. Experimental data (Riglet-Martial et al., 2014) are compared to predictions by the mass-action-law model. See text for explanations.

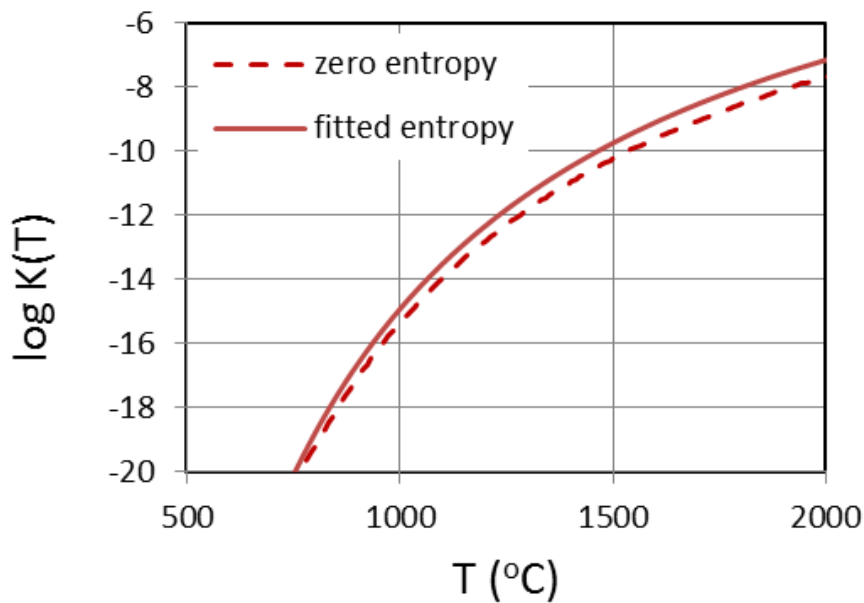


Fig.7 – Equilibrium constants calculated from eq. (9) assuming a zero entropy term (broken line) and $\Delta S_r/k_b = 1.4$ (continuous line), corresponding to the Cr mole fraction curves shown in Fig. 6.

Table 4 – Summary of thermodynamic data for the mass-action-law model of Cr(III) defects in UO_2 developed from reaction (1). The entropy was derived by fitting experimental Cr-solubility data from the literature. These data are used to calculate equilibrium constants for the defect reaction (1).

Function	[eV/defect]	[J mol ⁻¹]	Comment
ΔH_r	+ 3.05	294'281	from Middleburgh et al. (2012)
ΔS_r	1.21×10^{-4}	11.64	Calculated from $\Delta S_r/R=1.4$ (value fitted to Cr-solubility data compiled in Riglet-Martial et al., 2014)

Our predictions of Cr(III) equilibrium concentrations in stoichiometric UO_2 , based on the enthalpy determined via DFT by Middleburgh et al. (2012) appear to be fairly consistent with experimental Cr-solubility data, considering that the entropy correction required is small and well within the range of values observed for this kind of substitutions. For a typical fuel sintering temperature of 1800 °C we derive a solubility of about 0.6 mol% Cr(III) in UO_2 , consistent with the upper limit of 1'000 ppm (= 0.52 mol % Cr) imposed in the synthesis according to the ADOPT process (Arborelius et al. 2006).

An important consequence of the calculated solubility curve (cf. Fig. 6) is that extensive exsolution of Cr_2O_3 should occur during irradiation in the peripheral pellet regions since the Cr(III) solubility in UO_2 is predicted to fall below 0.02 mol% at reactor operation temperatures (< 1'000 °C). Whether this happens or not will also depend on thermal diffusion kinetics of Cr dissolved in UO_2 and on deviation from stoichiometry.

4 Development/application of a solid solution model for Cr-doped UO₂.

4.1 Preliminary remarks

In the first reporting year (see deliverable D1.10), preliminary oxygen potential calculations for a model fuel composition were carried out based on an *ideal* solid solution model defined with Cr(III)O_{3/2}, U(IV)O₂ and U(V)O_{2.5} end-members. From the data summarized in Table 4 and the low measured Cr-solubilities, it is, however, evident that incorporation of Cr(III) in UO₂ has a large positive enthalpy of mixing, which is not surprising considering the charge and ionic size mismatch of Cr³⁺ and U⁴⁺. Therefore, Cr(III) will form a strongly *non-ideal* solid solution with UO₂ and large positive mixing parameters for Cr/U interactions are expected.

In this section, we first define the end-members of a ternary solid solution in the system Cr(III)-U(IV)-U(V)-O according to the substitution mechanisms identified in the preceding Section as the energetically most favourable (defect reactions 1, 4 and 6). Then, we fit interaction parameters assuming a Berman-type solid solution model, using published experimental data on Cr-solubility in UO₂ and on hyperstoichiometry in the Cr-free U(IV)-U(V)-O system (*p*O₂ vs. O/U ratios). Finally, the calibrated solid solution model is implemented in GEM-Selektor and applied to calculate global chemical equilibrium under in-pile conditions for Cr-doped and conventional UO₂ fuels.

4.2 Definition of end-members

Fig. 8 shows the compositional space of the Cr-U(IV)-U(V)-O system. The selected end-member stoichiometries of the ternary solid solution are defined by the corners of the red triangle, besides alternative stoichiometries for the U(V) end-member that have been discarded. Both *bulk stoichiometries* (bold) and *site stoichiometries* (enclosed in square brackets) are given. UO_{2.5}, the end-member used in the preliminary calculations presented in Deliverable 1.10, was discarded since the thermodynamic data (and even the structure) of this phase are highly uncertain. UCrO₄ would be an adequate U(V) end-member. An orthorhombic compound with this stoichiometry is known, but its thermodynamic standard state properties are largely unknown.

As a consequence, we use the mixed U(IV)/U(V) stoichiometry U₄O₉ as U(V) end-member. This choice can be justified as follows: (a) the thermodynamic properties of U₄O₉ compounds are well-known over the whole temperature range of interest (Guillamont et al. 2003; Cordfunke and Konings, 1990); (b) the structures of all three polymorphs (α, β, γ -U₄O₉) are closely related to the fluorite-type UO₂ lattice (Bevan et al, 1986 ; Desgranges et al., 2011).

In Fig. 8, square brackets indicate *site stoichiometries* showing the occupancies of all moieties considered (Cr³⁺ U⁴⁺, U⁵⁺ and vacancies 'v') in all three sublattices (cationic, anionic, interstitial). For instance, the site formula of the U(V) end-member with bulk stoichiometry $\frac{1}{2}(\text{U}_4\text{O}_9)$, equivalent to 2(UO_{2.25}) or U₂O_{4.5}, readily shows that the cationic sublattice is half occupied by U⁴⁺ and half by U⁵⁺ cations, the anionic sublattice is fully filled by O²⁻ ions and the vacancy sublattice half-filled with O²⁻ ions, the other half remaining vacant.

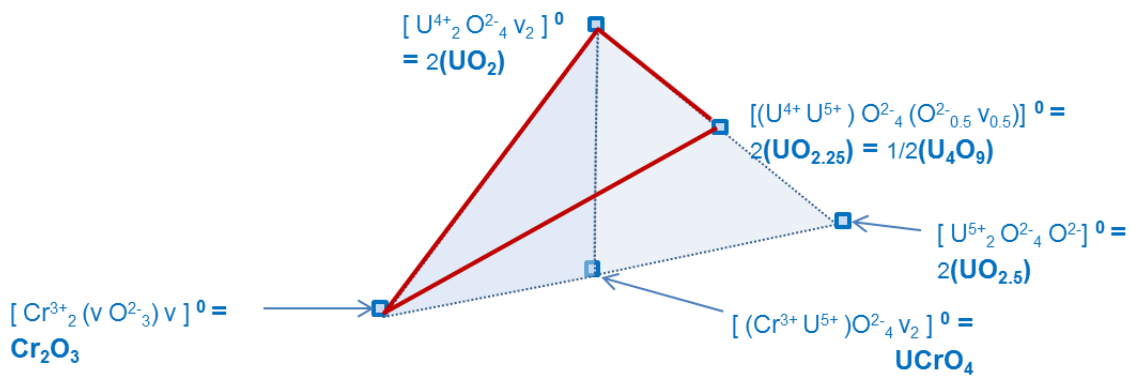


Fig. 8 - Compositional diagram of the U-Cr-O system showing the selected end-member stoichiometries (red triangle). The blue triangles indicate discarded alternatives (see text).

4.3 Implementation in GEM-Selektor and model calibration

This site notation is consistent with the mixing model of Berman and Brown (1984), which we adopt here to formulate the Cr(III)-U(IV)-U(V)O_{2+y} solid solution in GEM-Selektor. This model, originally developed to describe solid solutions and melts, allows treating vacancies as mixing moieties as well as the definition of partially occupied end-members. For this reason, it is preferred to a more rigorous Compound Energy Formalism (CEF) (Hillert, 2001). For instance, it would not be possible to define U₄O₉ as end-member with the CEF model because the cationic sublattice is occupied by two mutually mixing species (U⁴⁺ and U⁵⁺). CEF requires end-members in which each site is fully occupied by a single species. This would be appropriate for systems with a large and complete set of experimental data that allow simultaneous fitting of a large number of interaction parameters. We are, unfortunately, not in such a position.

The interaction parameter table of the Berman-type non-ideal Cr(III)-U(IV)-U(V)O_{2+y} solid solution (corresponding to the red triangle in Fig. 8) is shown in Fig. 9 as it is formulated in GEM-Selektor. Eleven pseudo-ternary interaction parameters were defined, each allowing for the definition of three coefficients describing temperature dependence. It turned out that three non-zero parameters with a single coefficient (as indicated in Fig. 9) are sufficient to fit all experimental data used to calibrate the model (see later).

In order to determine the parameter $W_{Cr-U4-U4}$, which describes interaction of trace amounts of Cr with almost pure UO₂, we resorted to the same Cr-solubility data (Riglet-Martial et al., 2014) used earlier for the determination of the defect formation entropy. These data, obtained in the temperature range 1500-1760 °C, are shown in Fig. 10 as mole fractions of Cr in UO₂ as a function of the measured equilibrium pO_2 . Corresponding best fit calculations are shown as lines with colours corresponding to the data for a specific temperature. Each line is obtained from a series of GEM-Selektor calculations (typically 50) in which the amount of O₂ in a closed system containing 1 mole of UO₂ and a small excess of metallic Cr is progressively

increased. The lines define the $\log p_{\text{O}_2}$ – Cr mole fraction values for the solid solution in equilibrium either with metallic Cr (to the left of the sharp kink) or with pure Cr_2O_3 (to the right of the kink).

	ipic1	ipxT	ipxT	ipxT	ipxT	ph cf[0]	ph cf[1]	ph cf[2]
0	W_Cr_Cr_U4	0	5	5	1	0	0	0
1	W_Cr_Cr_U5	0	5	5	0	0	0	0
2	W_Cr_U4_U4	0	5	1	1	255000	0	0
3	W_Cr_U5_U5	0	5	0	0	0	0	0
4	W_U4_U5_U5	0	1	0	0	100000	0	0
5	W_U4_U4_U5	0	1	1	0	100000	0	0
6	W_Cr_U4_U5	0	5	1	0	0	0	0
7	W_O1_O1_Va1	1	2	2	6	0	0	0
8	W_O1_Va1_Va1	1	2	6	6	0	0	0
9	W_Va2_Va2_O2	2	3	3	4	0	0	0
10	W_Va2_O2_O2	2	3	4	4	0	0	0
						w1	w2	w3

Fig. 9 - Screenshot from GEM-Selektor thermodynamic data input, showing the interaction parameter table for the non-ideal Cr-UO_{2+y} solid solution after calibration.

The optimized $W_{\text{Cr}_U4_U4}$ values in J/mol are indicated in the legend of Fig. 10. It is evident that high positive parameters are required to fit the very low measured Cr-solubilities in UO_2 (between 0.1 and 1 mol %). The ideal solid solution model predicts equilibrium mole fractions of Cr in UO_2 that are greatly in excess of the experimental data and is therefore inadequate. The fitted $W_{\text{Cr}_U4_U4}$ -values are remarkably independent of temperature, as indicated by the low standard deviation of the calculated average (261.8 ± 6.6 kJ/mol). Taking into account a possible slight increase at $T \geq 1700$ °C, we decided to adopt the value of 255 kJ/mol obtained at 1500 °C, which is comparable to central pellet temperatures during irradiation in commercial LWRs.

The fitted values of the $W_{\text{Cr}_U4_U4}$ mixing parameter (261.8 ± 6.6 kJ/mol) is close to the value inferred atomistically by Middleburgh et al. (2013) for the energy of dissolution of Cr(III) in UO_2 ($\Delta H_r = 294.3$ kJ/mol, see Table 4).

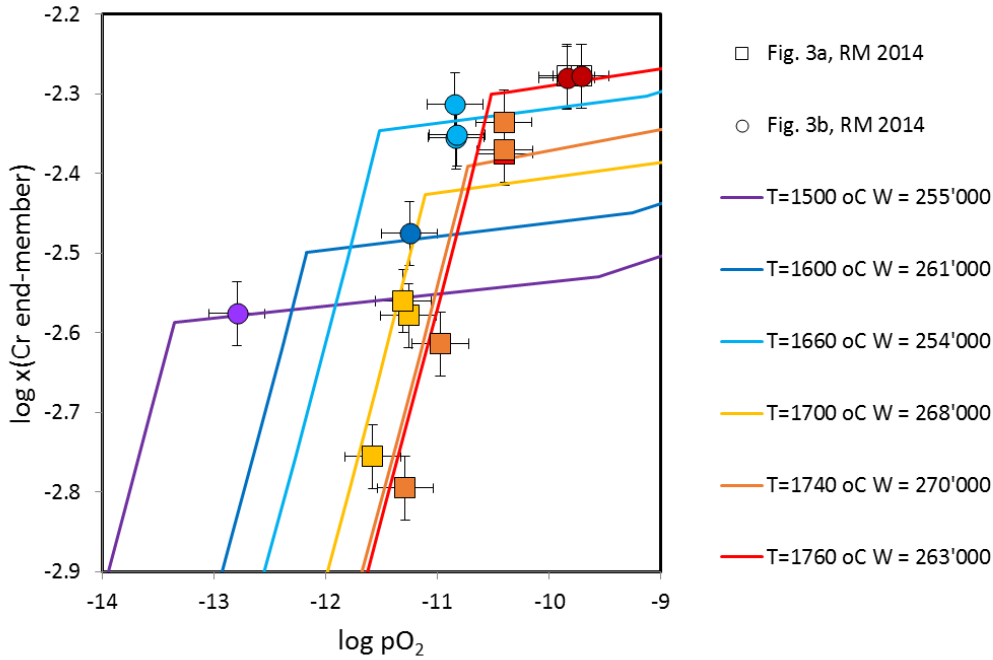


Fig. 10 - Determination of $W_{Cr_U4_U4}$ mixing parameter: Cr-solubility data from Riglet-Martial et al. (2014) are fitted by trial and error via GEM-Selektor calculations. The sharp kinks in the model curves correspond to the transition from Cr metal to Cr_2O_3 stability field for the specific temperature.

Nakamura and Fujino (1987) report over a wide temperature range (500 – 1100 °C) experimental values of oxygen equilibrium partial pressures in equilibrium with urania, as a function of the hyperstoichiometry coefficient y in UO_{2+y} . These measurements constitute an important data set for calibrating the $(UO_2)_2$ - $(UO_{2.25})_2$ binary of our solid solution model. We first attempted a global fitting by varying simultaneously several interaction parameter combinations. This was done using the GEMSFIT package (Miron et al., 2015) a specialized software, which runs systematically GEM equilibria calculations and seeks for optimized values of predefined parameter sets.

In our case, up to four interaction parameters, to which results proved to be sensitive, were varied simultaneously. After a large number of attempts, it turned out that it is not possible to find a *single* combination of interaction parameters capable of fitting the ensemble of the data. We however succeeded in finding *two* distinct combinations, one fitting satisfactorily the low-hyperstoichiometry region ($y < 0.02$), the other fitting the high hyperstoichiometry region ($y > 0.02$).

Because off-stoichiometry of irradiated UO_2 fuels does not exceed a few permils (Spino and Peerani 2008 and references therein) application of the low-hyperstoichiometry parameter set is sufficient. We finally obtained a simple combination ($W_{U4_U5_U5} = W_{U4_U5_U5} = 100$ kJ/mol, see Fig. 9) that reproduces reasonably well all data at $y < 0.02$ at all temperatures, as shown in Fig. 11.

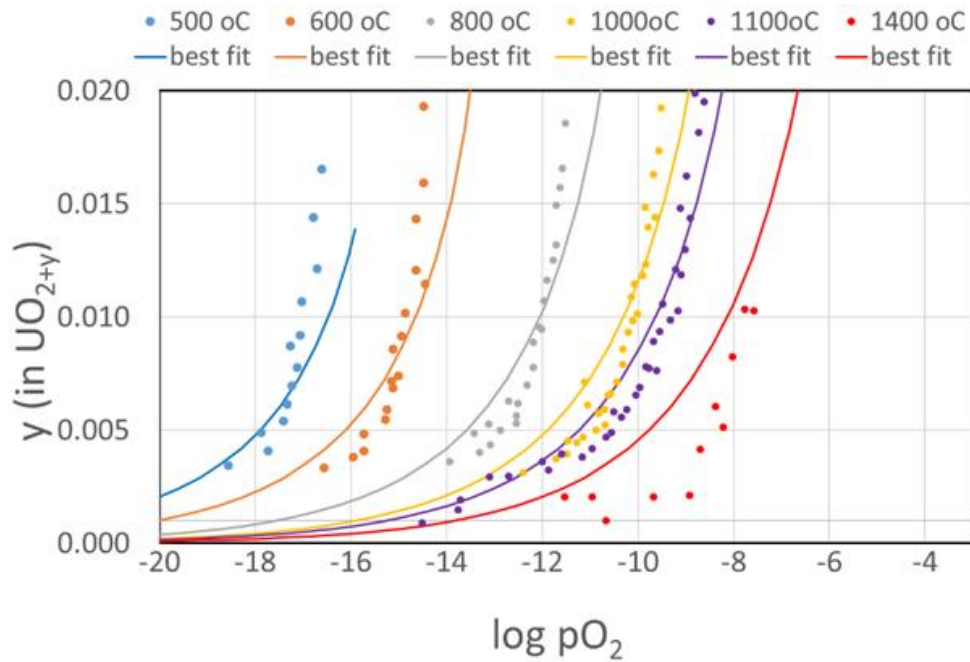


Fig. 11 - Determination of interaction parameters for the low hyperstoichiometry region of the $(\text{UO}_2)_2$ - $(\text{UO}_{2.25})_2$ binary by fitting the data given in Nakamura and Fujino (1987).

4.4 Fuel oxygen potential calculations

In this Section, thermodynamic calculations applied to model fuels are presented and discussed. These systems are equilibrated with the previously discussed Cr-doped UO_{2+y} solid solution, alternatively assuming ideal mixing (interaction parameters set to zero) and non-ideal mixing (optimized interaction parameters). Fission products and actinides other than uranium are modelled through equilibrium with pure oxides or metallic phases and the gas is treated as ideal mixture at 1 bar. From the results of the GEM-Selektor/HERACLES calculations, $p\text{O}_2$ and oxygen potential values could be readily extracted.

Calculations were carried out both for conventional UO_2 fuel and for an equivalent fuel doped with 1 mol % Cr(III) added as oxide. The composition of the non-doped fuel was taken from the model inventory specified in Table XV of Ferry et al. (2004), which refers to a 60 GWd/t_{HM} LWR 2 years after discharge. Some simplifications were required since the HERACLES thermodynamic database does not include all the listed elements. For instance, the inventories of a number of lanthanides (Pm, Sm, Gd, Tb, Dy, Ho) were assigned in equal proportions to the La and Nd inventories. The composition of the equivalent doped fuel was obtained simply by replacing 1 mol % of the initial UO_2 with $\text{CrO}_{1.5}$ and reducing the amounts of fission products, Pu and minor actinides proportionally to the “subtracted” U.

Fig. 12a shows the results of two distinct fuel oxygen potential calculations for the Cr-doped model fuel. The first (broken blue line, “niSS”) was obtained by equilibrating the non-ideal Cr(III)- UO_{2+y} solid solution with the optimized interaction parameters described in the previous

section, the second (turquoise continuous line, “idSS”) was computed assuming ideality, i.e. setting all interaction parameters to zero. Fig. 12b is simply a zoom of the high-temperature high- ΔGO_2 region of Fig. 12a.

At high temperatures, the calculations yield slightly lower (more negative) oxygen potentials in the case of ideal mixing. Overall, the differences are surprisingly small (less than 5 kJ/mol). The oxygen potential calculated assuming equilibrium with the non-ideal solid solution coincides exactly with the oxygen potential calculated for a mixture of pure metallic Mo and pure Mo(IV)O₂ in mutual equilibrium, except at the highest temperatures, where it joins the ideal solid solution (idSS) model curve.

The slightly lower potentials calculated for the ideal solid solution (‘idSS’) model are due to the higher oxygen content (and thus higher hyperstoichiometry) required by an ideal Cr(III)-UO_{2+y} solid solution compared to the non-ideal solid solution. Suppressing the strongly positive U(IV)/U(V) interaction parameters implies that more oxygen is stored in the ideal solid solution phase. The excess oxygen incorporated in the ideal Cr(III)-UO_{2+y} solid solution is then not available to the redox species “outside” the UO_{2+y} phase. This destabilizes Mo(IV)O₂ and thus leads to the breakdown of the Mo/MoO₂ buffer at comparatively low temperatures. As a result, lower fuel oxygen potentials are obtained compared to the more realistic calculation with optimized interaction parameters. The described effects are, however, minor, and both curves cross the field defined by ΔGO_2 measurements of LWR fuels by Matzke (1995).

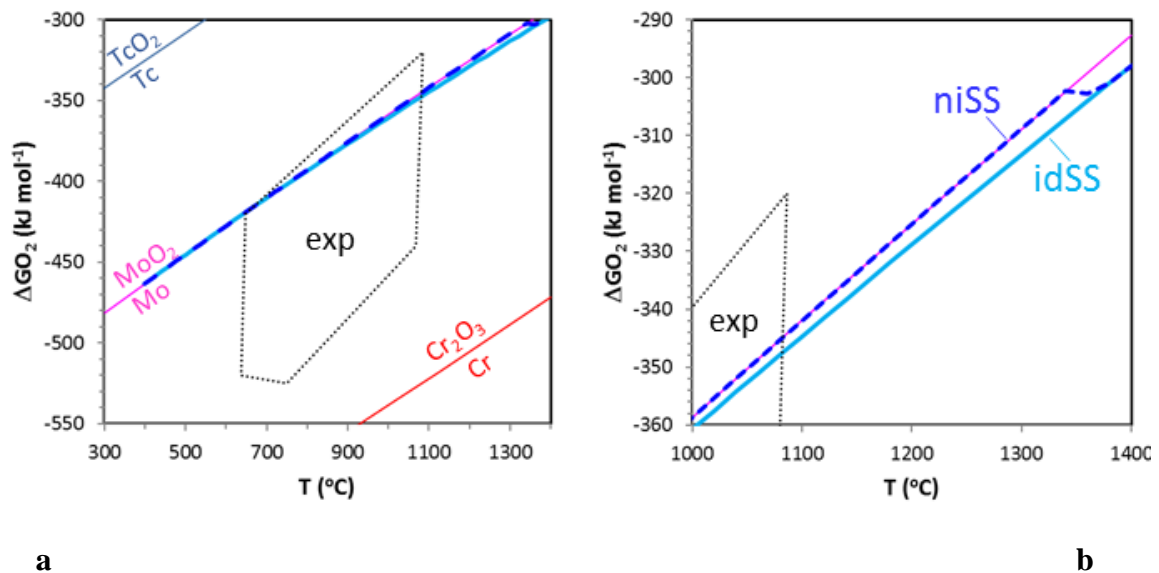


Fig. 12 - Calculated oxygen potentials of Cr-doped fuels compared to equilibria of coexisting pure metal/oxide pairs (left: overview; right: detail). The area denoted ‘exp’ is the region of measured oxygen potentials for LWR fuels up to 58 GWd/t_{IHM} (Matzke, 1995). The ‘niSS’ curve was calculated using optimized interaction parameters for the non-ideal Cr(III)UO_{2+y} solid solution. The ‘idSS’ is the equivalent prediction assuming ideal mixing.

An equivalent calculation (not shown in Fig. 12) for *non-doped* UO₂ fuel, using the optimized non-ideal solid solution, yielded indistinguishable results, i.e. identical oxygen potentials were calculated for non-doped and Cr-doped UO₂ fuel. Because the assumed doping level (1 mol % Cr) ensured that chromium solubility in urania was always reached at all temperatures of interest (400-1400 °C), these results suggest that Cr-doping should not affect significantly the oxygen potential of the fuel. This conclusion is however not definitive, since the current thermodynamic model for the fuel system is far from being complete and requires further implementations (see next Section).

4.5 Outlook

The model presented here still needs improvements that we will implement and finalize during the next project year. The solid solution model defined for the UO₂ phase is not yet complete, since it does not account for incorporation of a number of elements known to be soluble in the matrix phase (Pu, minor actinides and lanthanides). Moreover, additional solid solution phases form during irradiation, particularly an intermetallic phase (ϵ -particles) dominated by Mo, Ru, Tc, Pd, Rh and the “grey phase”, a perovskite-type multicomponent phase with (Ba,Sr)(Zr,U,Mo)O₃ stoichiometry. Within the limits of feasibility allowed by the available experimental data, we will introduce these two solid solution phases. Finally, the calculations presented in this report refer to end-of-cycle conditions. We plan, therefore, to carry out calculations related to the oxygen potential evolution with increasing burnup, also taking into account partial internal oxidation of the Zircaloy cladding.

References

- Arborelius J., Backman K., Hallstadius L., Limbäck M., Nilsson J., Rebensdorff B., Zhou G., Kitano K., Löfström R. and Rönnberg G. (2006) Advanced Doped UO₂ Pellets in LWR Applications. *J. Nucl. Sci. Technol.* 43(9), 967–976.
- Barin I.B. (1989) Thermodynamic data of pure substances, VCH Verlagsgesellschaft mbH, 0-6940 Weinheim (Vol. 1, pp. 418 ff).
- Berman R.G. and Brown T.H. (1984) A thermodynamic model for multicomponent melts, with application to the system CaO-Al₂O₃-SiO₂. *Geochim. Cosmochim. Acta* 48, 661-678.
- Bevan D.J.M., Grey I.E. and Willis B.T.M. (1986) The crystal structure of β -U₄O_{9-y}. *J. Solid State Chem.* 61, 1-7.
- Bourgeois L., Dehaut Ph., Lemaignan C. and Hammou A. (2001), Factors governing microstructure development of Cr₂O₃-doped UO₂ during sintering. *J. Nucl. Mater.* 297, 313–326.
- Cordfunke E.H.P. and Konings R.J.M. (1990) Thermochemical data for reactor materials and fission products. North Holland, Amsterdam.
- Cox J.D., Wagman D.D. and Medvedev V.A. (1989) CODATA Key Values for Thermodynamics, Hemisphere Publishing Corp., New York.
- Desgranges L., Baldinozzi G., Siméone D. and Fischer H.E. (2011) Refinement of the α -U₄O₉ Crystalline Structure: New Insight into the U₄O₉ - U₃O₈ Transformation. *Inorg. Chem.* 50, 6146–6151.
- Elorrieta J.M., Bonales L.J., Rodriguez-Villagra N., Baonza V.G. and Cobos J. (2016) A detailed Raman and X-ray study of UO_{2+x} oxides and related structure transitions. *Phys. Chem. Chem. Phys.*, 18, 28209-28216.
- Ferry C., Poinssot, Ch., Broudic V., Cappelaere Ch., Desgranges L., Garcia Ph., Jégou Ch., Lovera P., Marimbeau P., Piron J.-P., Poulesquen A. and Roudil D. (2004) Synthesis on the long term spent fuel evolution. Report CEA-R-6084. Commissariat à l’Energie Atomique (CEA), France.
- Garcia Ph., Pizzi E., Dorado B., Andersson D., Crocombette J.-P., Martial Ch., Baldinozzi G., Siméone D., Maillard S. and Martin G. (2017) A defect model for UO_{2±x} based on electrical conductivity and deviation from stoichiometry measurements. *J. Nucl. Mat.* 494, 461-472.
- Goff J.P., Hull S., Hutchings M.T. and Clausen K.N. (1999) Defect structure of yttria-stabilized zirconia and its influence on the ionic conductivity at elevated temperatures. *Phys. Rev. B* 59(22), 14 203 – 14 219.
- Guillaumont R., Fanghänel T., Neck V., Fuger J., Palmer D.A., Grenthe I. and Rand M.H. (2003) Update on the Chemical Thermodynamics of Uranium, Neptunium, Plutonium,

Americium and Technetium, F.J. Mompean et al. Eds., Chemical Thermodynamics Vol. 5, Nuclear Energy Agency, Elsevier, Amsterdam, 918 p.

Guo Z., Ngayam-Happy R., Krack M. and Pautz A. (2017) Atomic-scale effects of chromium-doping on defect behaviour in uranium dioxide fuel. *J. Nucl. Mat.* 488, 160-172.

Hillert M. (2001) The compound energy formalism. *J. Alloys Compounds* 320, 161-176.

Jeannin Y., Mannerskantz C. and Richardson F.D. (1963) Activities in Iron-Chromium Alloys. *Transactions of the Metallurgical Soc. AIME*, 227, 300-305.

Kulik D.A., Wagner T., Dmytrieva S.V., Kosakowski G., Hingerl F.F., Chudnenko K.V., Berner U. (2013): GEM-Selektor geochemical modeling package: revised algorithm and GEMS3K numerical kernel for coupled simulation codes. *Computational Geosciences* 17, 1-24.

Leenaers A., de Tollenaere L., Delafoy Ch. and Van den Berghe S. (2003) On the solubility of chromium sesquioxide in uranium dioxide fuel. *J. Nucl. Mater.* 317, 62–68.

Matzke H. (1995) Oxygen potential measurements in high burnup LWR UO₂ fuel. *J. Nucl. Mat.* 223, 1-5.

Middleburgh S.C., Parfitt D.C., Grimes R.W., Dorado B., Bertolus M., Blair P.R. Hallstadius, L. and K. Backman (2012) Solution of trivalent cations into uranium dioxide. *J. Nucl. Mat.* 420, 258–261.

Mieszczynski C., Kuri G., Bertsch J., Martin M., Borca C.N., Delafoy Ch. and Simoni E. (2014) Microbeam x-ray absorption spectroscopy study of chromium in large-grain uranium dioxide fuel. *J. Phys.: Condens. Matter* 26, 355009.

Miron G.D., Kulik D.A., Dmytrieva S.V. and Wagner T. (2015) GEMSFITS: Code package for optimization of geochemical model parameters and inverse modeling.

Motta A.T. and Olander D.R. (2017) *Light Water Reactor Materials*, Vol. 1, chapter 4. American Nuclear Society. ISBN-13: 978-0894484612.

Nakamura A. and Fujino T. (1987) Thermodynamic study of UO_{2+x} by solid state EMF technique. *J. Nucl. Mat.* 149, 80-100.

Olander D.R. (1976) *Fundamental aspects of nuclear reactor fuel elements*. National Technical Information Service, U. S. Department of Commerce, Springfield, Virginia 22161, 613 p.

Parkes M.A., Refson K., d’Avezac M., Offer G.J., Brandon N.P. and Harrison N.M. (2015) Chemical Descriptors of Ytria-Stabilized Zirconia at Low Defect Concentration: An ab Initio Study *J. Phys. Chem. A* 119, 6412–6420.

Pauling L. (1929). The principles determining the structure of complex ionic crystals. *J. Am. Chem. Soc.* 51 (4), 1010–1026.

Pearson R.G. (1968) Hard and soft acids and bases, HSAB, part 1: Fundamental principles. *J. Chem. Educ.* 1968 (45), 581–586.

Povoden E., Grundy A.N. and Gauckler L.J. (2006) Thermodynamic Reassessment of the Cr-O System in the Framework of Solid Oxide Fuel Cell (SOFC) Research. *Journal of Phase Equilibria and Diffusion*, 27(4), 353-362.

Prieur D., Martin Ph., Lebreton F., Delahaye Th, Banerjee D., Scheinost A.C., Jankowiak A. (2013) Accommodation of multivalent cations in fluorite-type solid solutions: Case of Am-bearing UO_2 . *J. Nucl. Mat.* 434, 7-16.

Prieur D., Martel L., Vigier J.-F., Scheinost A.C., Kvashnina K.O., Somers J. and Martin Ph. (2018) Aliovalent Cation Substitution in UO_2 : Electronic and Local Structures of $\text{U}_{1-y}\text{La}_y\text{O}_{2\pm x}$ Solid Solutions. *Inorg. Chem.* 57, 1535-1544.

Riglet-Martial Ch., Martin Ph., Testemale D., Sabathier-Devals C., Carlot G., Matheron P., Iltis X., Pasquet U., Valot C., Delafoy C. and Largenton R., Thermodynamics of chromium in UO_2 fuel: A solubility model, *J. Nucl. Mat.* 447, 63–72.

Shannon R.D. (1976) Revised effective ionic radii and systematic studies of interatomic distances in halides and chalcogenides. *Acta Cryst.* A32, 751-767.

Smyth D.M. (2000) The defect chemistry of metal oxides. Oxford University Press, New York & Oxford, 294 p.

Spino J. and Peerani P. (2008) Oxygen stoichiometry shift of irradiated LWR-fuels at high burn-ups: Review of data and alternative interpretation of recently published results. *J. Nucl. Mat.* 375, 8-25.

Stubican V. S. and Greskovich C. (1975) Trivalent and divalent chromium ions in spinels. *Geochim. Cosmochim. Acta* 39, 375-881.

Toker N.Y., Darken L.S. and Muan A. (1991) Equilibrium Phase Relations and Thermodynamics of the Cr-O System in the Temperature Range of 1500 °C to 1825 °C. *Metallurgical Trans. B*, 22B, 225-232.

Yu J., Bai X.-M., El-Azab A. and Allen T.R. (2015) Oxygen transport in off-stoichiometric uranium dioxide mediated by defect clustering dynamics. *The Journal of Chemical Physics* 142, 094705.

Wang J., Ewing R.C. and Becker U. (2014) Average structure and local configuration of excess oxygen in UO_{2+x} . *Scientific Reports* 4:4216.

Willis B.T.M. (1978) The defect structure of hyperstoichiometric uranium dioxide. *Acta Cryst.* A34, 88-90.

Appendix 1 – Calculation of Cr(III) solubility in UO₂ based on defect equilibria

In order to determine the solubility of Cr(III) in stoichiometric UO₂ (synthesis conditions) one starts by defining appropriate equations following the rules of defect equilibria (Smyth, 2000; Motta and Olander, 2017):

$$\text{Constant lattice site ratio: } N_O = 2N_U = 2N_i \quad (\text{A1.1})$$

$$\text{U site mass balance: } N_U = n_{U\bar{U}} + n_{Cr'_U} \quad (\text{A1.2})$$

$$\text{O site mass balance: } N_O = n_{O\bar{O}} + n_{v''_O} \quad (\text{A1.3})$$

$$\text{Electroneutrality: } 4 n_{U\bar{U}} + 3 n_{Cr'_U} = 2 n_{O\bar{O}} \quad (\text{A1.4})$$

where N stays for the total amounts of lattice sites (moles or number of site) and n denotes the amounts actually occupied by the defect species defined in the subscripts. The subscripts O , U and i denote uranium, oxygen and interstitial sites, respectively. Using (A1.1) and dividing (A1.2), (A1.3) and (A1.4) by N_U , one obtains corresponding equations expressed in terms of mole fractions normalized to the total amount of U sites:

$$\text{U site mass balance: } 1 = x_{U\bar{U}} + x_{Cr'_U} \quad (\text{A1.2a})$$

$$\text{O site mass balance: } 2 = x_{O\bar{O}} + x_{v''_O} \quad (\text{A1.3a})$$

$$\text{Electroneutrality: } 4 x_{U\bar{U}} + 3 x_{Cr'_U} = 2 x_{O\bar{O}} \quad (\text{A1.4a})$$

The exact equilibrium constant for the Cr-substitution in stoichiometric according to reaction (1), reported in Section 3.3, is given by:

$$K(T) = \frac{x_{Cr'_U}^2 x_{v''_O}}{x_{U\bar{U}}^2 x_{O\bar{O}}} \cong x_{Cr'_U}^2 x_{v''_O} \quad (\text{A1.5})$$

The approximation made in (A1.5) is valid for very low concentrations of defects, which applies to most defect equilibria. Defining

$x_{U\bar{U}} \equiv x$, $x_{Cr'_U} \equiv y$, $x_{O\bar{O}} \equiv u$, $x_{v''_O} \equiv z$, we rewrite eqs. (A1.2a) to (A1.5) as follows:

$$\text{U site mass balance: } 1 = x + y \quad (\text{A1.2a})$$

$$\text{O site mass balance:} \quad 2 = u + z \quad (\text{A1.3a})$$

$$\text{Electroneutrality:} \quad 4x + 3y = 2u \quad (\text{A1.4a})$$

$$\text{Cr defect equilibrium:} \quad K = y^2 z \quad (\text{A1.5a})$$

The solution of this system of equation yields:

$$x_{U^x} = 1 - \sqrt[3]{2K(T)} \quad (\text{A1.2b})$$

$$x_{Cr^I} = \sqrt[3]{2K(T)} \quad (\text{A1.3b})$$

$$x_{O^x} = 2 - \frac{\sqrt[3]{2K(T)}}{2} \quad (\text{A1.4b})$$

$$x_{V^{\circ}} = \frac{\sqrt[3]{2K(T)}}{2} \quad (\text{A1.5b})$$